Research Square

Preprints are preliminary reports that have not undergone peer review.
They should not be considered conclusive, used to inform clinical practice,
or referenced by the media as validated information.

Numerical study on the effect of blank-holding techniques on the countersinking process

Hassen Mosbah

hassen.mosbah@yahoo.fr

ISET Gafsa: Institut Superieur des Etudes Technologiques de Gafsa

Slimen Attyaoui

Rachid Nasri

Research Article

Keywords: countersinking, metal forming, blank-holder, progressive force, forming kinematics, finite elements

Posted Date: September 14th, 2026

DOI: https://doi.org/10.21203/rs.3.rs-10864761/v1

License: This work is licensed under a Creative Commons Attribution 4.0 International License.
Read Full License

Numerical study on the effect of blank-holding techniques on the countersinking process

Hassen Mosbah[1], Slimen Attyaoui[2] and Rachid Nasri[3].

[1] *LR- MAI-11-ES19-ENIT, Institut supérieur des études technologiques de Gafsa (ISET Gafsa)*
[2] *LR- MAI-11-ES19-ENIT, École Nationale d'ingénieurs de Carthage (ENICAR)*
[3] *LR- MAI-11-ES19-ENIT, École Nationale d'ingénieurs de Tunis (ENIT)*

**Corresponding author Email: hassen.mosbah@yahoo.fr*

Abstract

This work presents a comprehensive numerical study of the influence of blank holding on the countersinking process. This study evaluates three distinct blank holding methods. Firstly, an imposed displacement was applied to the blank holder. This model resulted in an excessive blank holder force (BHF). Within this model, a particular case featuring a null imposed displacement was explored, referred to as the maintained blank-holder model. This configuration served as a foundation for proposing two innovative models incorporating a progressive blank-holding force. These forces were produced by using an appropriate elastic annular ring. Furthermore, these two new models were implemented with and without a clearance between the blank-holder and the workpiece. Finite element simulations were performed using an elasto-plastic model to investigate the effects of these different types of blank-holding on the forming kinematics and the resulting forces. A comparative analysis revealed that the newly proposed progressive blank-holding forces significantly reduced geometric imperfections and the energy consumption during the countersinking process.

Keywords: *countersinking, metal forming, blank-holder, progressive force, forming kinematics, finite elements*

1. Definition

Countersinking is used widely in sheet metal forming. This process consists of enlarging a truncated pre-hole. The obtained internal shape is called a countersink, and it is used to locate a rivet or a screw head. In practice, the sheet metal used for countersinking is clamped around its periphery by a blank-holder, and a conical punch then applies concentrated deformation to enlarge the side of an existing pre-hole.

Recent research has focused on the fatigue life and cracking behaviour of joined assembly sheets using fasteners and countersunk holes. [1] studied the surface characteristics. Other researchers, such as [2], [3], [4], [5], and [6], studied the fatigue life of countersunk holes and riveted assemblies. [7] and [8] focused on cracking behaviour. [9] studied the characteristics of the riveted link. [10] studied the stress concentration factor in the countersunk hole.

Many other researchers focused on forming kinematics, the effects of the geometric parameters, and the optimization of the countersinking process. [11] studied the forming kinematics in the countersinking process. They developed a 2D asymmetric model with a nil-imposed displacement applied to the blank holder. They observed new forming kinematics in the countersinking process, such as gaps and expansions. After that, they investigated the loads during the process. They found that the blank holder reaction force had three stages during the process, which helped to explain the appearance and the evolution of many kinematic phenomena. In addition, they found that the pre-hole fillet of the workpiece influences the punch force. That's why it should be chosen with caution to obtain an experimental punch force curve that fits the numerical one.

[12] used a statistical method based on the new definitive screening design (DSD) to investigate the effects of the workpiece geometric parameters on the final shape of the countersunk hole. In this work, three parameters were adopted: the radius of the pre-hole and its fillet, as well as the thickness of the workpiece. They found that the pre-hole radius had the dominant effect on the shape of the countersunk hole and the punch force. They confirmed that the pre-hole fillet had a significant impact on the punch force, and the workpiece thickness influenced the height of the countersunk hole.

[13] developed an optimization methodology based on the RMS method coupled with design of experiments and the SQP algorithm. This work aims to find optimal parameters to obtain a normalized countersunk hole while preventing the knife-edge phenomenon. The adopted factors are the punch travel and the radius of the pre-hole. The results showed the ability of this method to determine optimal parameters.

In industry, the main concern is choosing a suitable press machine and controlling the BHF to obtain an optimal product by reducing imperfections and energy consumption. Many press machines are used to apply different types of BHF in many forming processes. Up to now, little literature has focused on studying the effect of BHF used in the countersinking process. [14] suggested using an imposed displacement of 1µm applied to the blank holder. In their study, they performed a parametric finite element analysis to investigate the forming kinematics during the countersinking process. The obtained BHF was about 53 kN, which was greater than the punch force (40kN). Thus, this blank-holding technique led to excessive energy consumption.

To resolve this problem and reduce energy consumption in the countersinking process, the use of progressive BHF seems to be a suitable solution when single-action machines are utilized.

In the present work, axisymmetric elasto-plastic finite element models were developed to investigate the influence of different blank-holding forces on the forming kinematics of the countersinking process. Three distinct cases were considered. The first case (C1) involved the application of an imposed displacement to the blank-holder. When this imposed displacement became zero, the blank-holder reaction force was determined and served as a foundational element for the development of subsequent cases. The second case (C2) used a progressive BHF with no clearance (C=0), while the third case (C3) incorporated a clearance (C≠0). These progressive forces were implemented using an elastic annular ring. Experiments were conducted to validate the simulation results, and good agreement was obtained.

The primary objectives of this study are twofold: to effectively control the BHF to determine the optimal progressive force, and to understand the forming kinematics during the forming process.

2. Finite element modelling

The finite element analysis of the countersinking process was performed after defining the material behaviour, tool parameters, workpiece parameters, and boundary conditions. The studied models were created using Abaqus/Standard®.

2.1.Parameters

In this study, the three cases used the same workpiece parameters before and after deformation. The geometrical parameters are illustrated in Fig.1 and listed in Table.1. For case (C1), the adopted parameters of the tools are presented in Fig.1 and defined in Table.2. Concerning the cases (C1) and (C2), an annular ring was used to obtain the progressive blank-holder force as shown in Fig.3. The geometrical and mechanical characteristics of the used ring are detailed in Table.2.

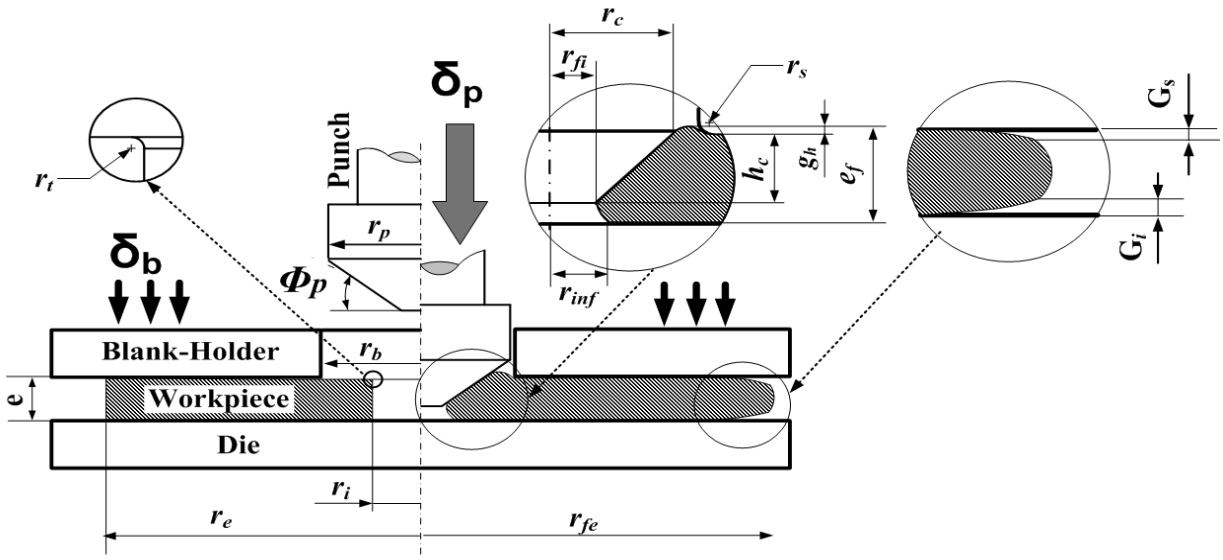


Fig.1 Parameters of the countersinking process

Table 1. Workpiece parameters

Parameters	*Symbol*	*Value*
Initial shape of the workpiece		
Initial internal radius	r_i	2.5-3 mm
Fillet radius of the pre-hole	r_t	0.1mm
Initial external radius	r_e	15 mm
Thickness	e	2.7mm
Final shape of the workpiece		
Final thickness	e_f	---------
Inferior gap	G_i	---------
Final internal radius	r_{fi}	---------
Final inferior hole radius	r_{inf}	---------
Final external radius	r_{fe}	---------
Superior radius of Countersink	r_c	---------
Height of Countersink	h_c	---------

Table 2. Parameters of tools and annular ring

Parameters	*Symbols*	*Values*
Tools		
Punch radius	r_p	5 mm
Punch angle	Φ_p	90°
Punch travel	δ_p	1.4 mm
Blank-Holder displacement	δ_b	--------
Blank-Holder inner radius	r_b	5 mm
Fillet radius of the BH hole	r_s	0.1 mm
Annular Ring		
Inner radius	r_1	5.5 mm
External radius	r_2	34 mm
Clearance	c	--------
Height	h	16 mm
Young's Modulus of annular ring	E_S	--------

2.2.Material behaviour

In this study, a 2.7-mm-thick S235 steel hot-rolled sheet was employed. In the countersinking proc$_{es}$s, the predominant stress state is one of compression. To characterize the material properties of the sheet metal, a uniaxial compression test was conducted, facilitating the derivation of the corresponding stress-strain curve as shown in Fig.2. This test was explained and detailed in the work of [15], [16], and [11]. The material was supposed to exhibit elasto-plastic behaviour and to obey the Von Mises yield criterion with an isotropic hardening rule. For the finite element models undertaken, a multi-linear uniaxial stress-strain law was implemented in Abaqus/Standard®. Utilizing a reverse methodology, the Young's modulus and yield stress were approximated at 210 GPa and 235 MPa, with Poisson's ratio assumed to be 0.3.

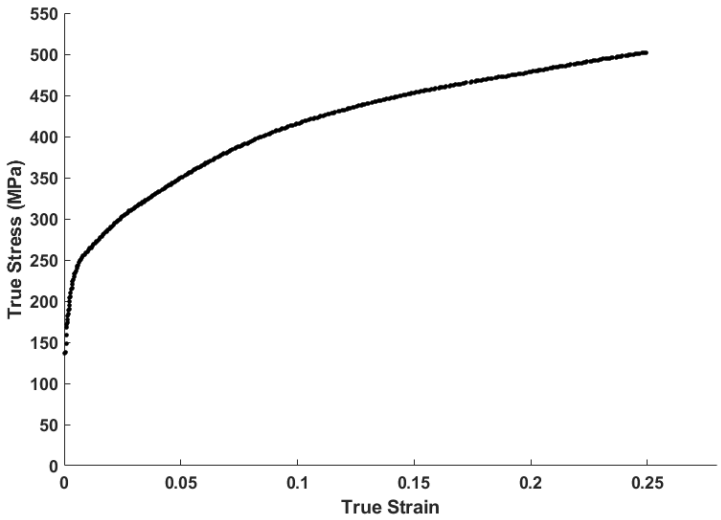


Fig.2 Experimental stress-strain curve

2.3.Finite element modelling and meshing

The studied models were created based on the geometries and dimensions of the experimental tools. For the first case (C1), an axisymmetric model was adopted as shown in Fig.1. The workpiece was modelled as a deformable body. Its material was assumed to exhibit elasto-plastic behaviour and obey the Von Mises yield-hardening rule. This workpiece was meshed using a 3-node linear triangle element (CAX3H) with reduced integration. To reduce error due to large plastic transformation, an adaptive process and a remeshing rule were used to refine the initial mesh. A typical workpiece mesh is presented in Fig.3. The blank-holder, die, and punch were modeled as axisymmetric rigid bodies.

The friction contact between the workpiece and the tools was modeled with Coulomb's friction law. Using reverse techniques, the friction coefficient was assumed constant at 0.12 to obtain reasonable contact conditions.

Concerning the models (C2) and (C3), the same model was adopted. Instead of imposing displacement on the blank holder, a progressive BHF was applied by using an annular ring fabricated with a suitable plastic material. This annular ring was positioned between the blank holder and punch, as shown in Fig.3. The upper face of the annular ring was fixed to the punch plate, and its lower face remained tangent to the blank-holder (C=0): it is case (C2). Case (C3) can be obtained from (C2) when the clearance becomes C≠0.

The annular ring was modeled as a deformable body and meshed using triangular elements (CAX3H). The contact between the ring and the tools was defined without friction. To avoid expansion of the annular ring, Poisson's ratio was set to zero ($\nu = 0$).

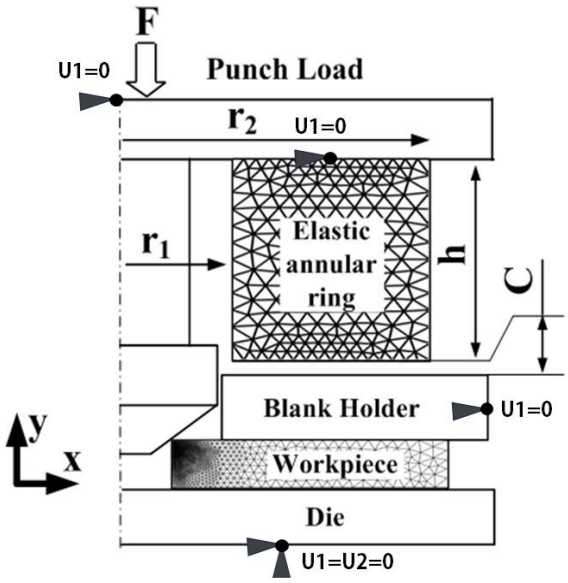


Fig.3 Axisymmetric model of the countersinking with annular ring: cases (C2) and (C3)

This annular ring has a stiffness K. It is defined by using the following equation:

$$K = \frac{\pi\left(r_2^2 - r_1^2\right).E_{spring}}{h} \qquad (1)$$

This stiffness K is proportional to E_S. In this study, the parameters r_1, r_2, and h are constant, as defined in Table.2. Thus, instead of referring to K, E_S will be used to represent the material selection for the associated stiffness. As a result, the next parametric study will be based on the choice of E_S.

2.4.Experimental tools

In this work, two experimental tools were used. The first tool is described in previous work [11], and it was used for case (C1). For the new cases (C2) and (C3), additional parts were used: a new blank-holder, annular ring, and shim. All parts were manufactured according to the developed finite element models, as shown in Fig.4.

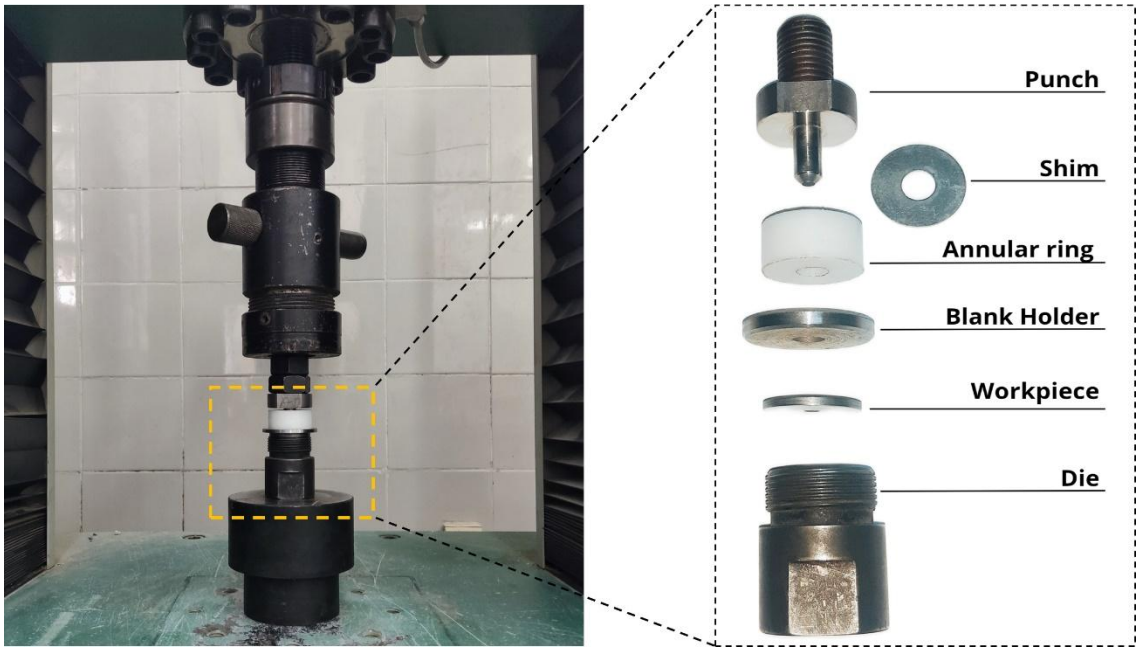


Fig.4 Experimental tools for case (C2) and (C3)

The experimental process is detailed as follows:

- The workpiece is a washed cut from the same sheet, with a thickness $e=2.7mm$ and an external diameter $r_e=30mm$. The inner diameter $r_i=5.4mm$ was obtained by drilling.
- A universal compression test machine of maximum capacity 200KN was used.
- The die, the workpiece, the annular ring, the blank-holder, the shim, and the punch were carefully placed coaxially to respect the same configuration as used in FE models. Shims with different thicknesses were used to get the desired clearance C.
- A preload of 200N was applied to move the punch down and to ensure the best contact between the punch and the workpiece. Then, this load was subtracted from the final results.
- The countersinking process was carried out with a controlled displacement and a constant speed of 5mm/min.

3. Results and discussions

3.1. Analysis of forming kinematics and loads for case (C1)

The study of model (C1) focused on load evolution during the process and the forming kinematics. Fig.5-a presents the evolution of retraction versus punch travel. It is clear that the greater the imposed displacement δ_b on the blank-holder, the greater the increase in retraction $(r_{fi}-r_i)$. An imposed displacement of $\delta_b=2\mu m$ increased the retraction by about 20% compared to the maintained configuration when $\delta_b=0\mu m$.

For a punch travel of δ_b=1mm, the retraction reached its maximum; however, the δ_p value. After that, it decreased and reached the final value.

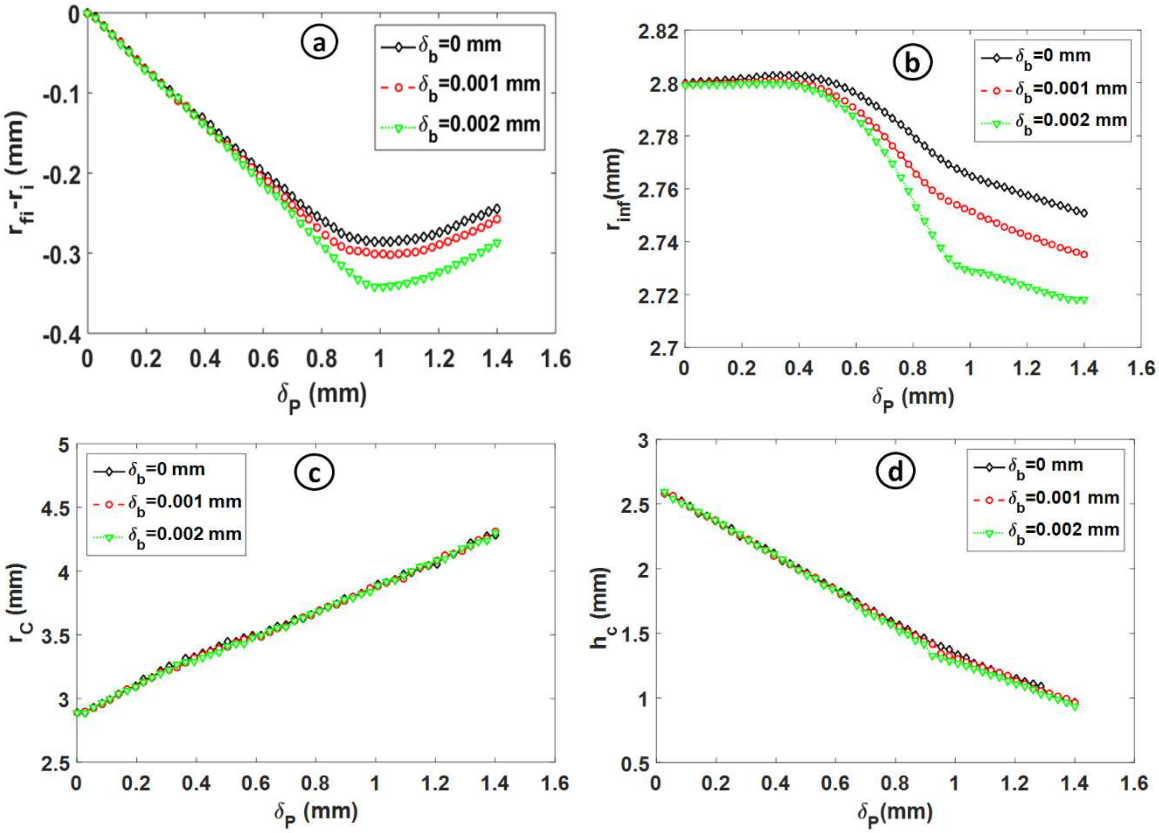


Fig.5 Evolution versus punch travel of: (a) Retraction, (b) R_{inf}, (c) r_C and (d) h_C , case (C1)

Fig.5-b shows that increasing the imposed displacement slightly increases the inner inferior diameter r_{inf} of the countersunk hole.

When the punch travel exceeded 1 mm, the inner hole was enlarged, and material flowed into the directions where there was no contact with the tools. As a result, the workpiece was expanded. The radial and axial expansion appeared clearly, as shown in Fig.5-c-d.

In addition, the imposed displacement variation did not affect the radial expansion $(r_{fe}-r_e)$, but its impact was clear on axial expansion, as observed in Fig.6-a-b. Concerning the gaps, it was observed that the superior gap had a negative value during the process, which led to a reduction of the workpiece thickness at the outer edge. It was noticed that the inferior gap was about 4 times greater than the superior gap. The evolution of these gaps and their final values were slightly affected by the imposed displacement applied to the blank-holder, as shown in Fig.6-c-d.

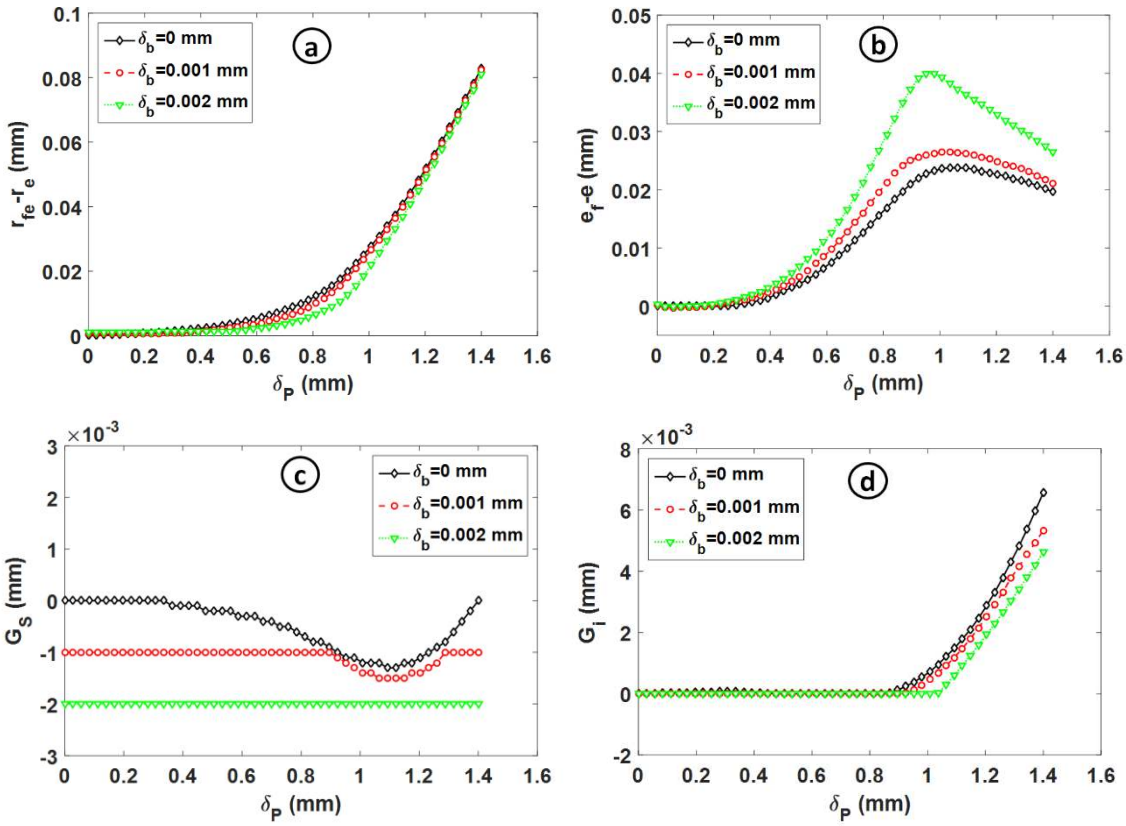


Fig.6 Evolution versus punch travel of: (a) Radial expansion, (b) Axial expansion, (c) G_S and (d) G_i, case (C1)

To better understand the influence of blank holding, the axial loads were plotted in Fig.7. The evolution of the punch load was quasi-linear, and its maximum value was obtained at the end of the process. As observed in Fig.7-b, the imposed displacement variation did not affect the evolution of the punch load during punch displacement.

The reaction force was measured as the blank-holder force in case (C1) when the imposed displacement is zero. In Fig.7-a, it can be observed that no reaction force appeared at the beginning of the process. After a punch travel of δ_b=0.45mm, the reaction force increased until the end of the process.

By applying an imposed displacement $\delta_b \neq 0$, the BHF appeared at the beginning of the process and with a high value. For case (C1), with $\delta_b = 2\mu m$, the maximum BHF is *120KN* which is 3 times greater than the maximum punch load (*41KN*).

As a consequence, the improper imposed displacement leads to an excessive BHF, which is greater than the necessary punch load for the process. It is the weak point of this kind of blank holding, since in manufacturing, the BHF must not exceed the punch load.

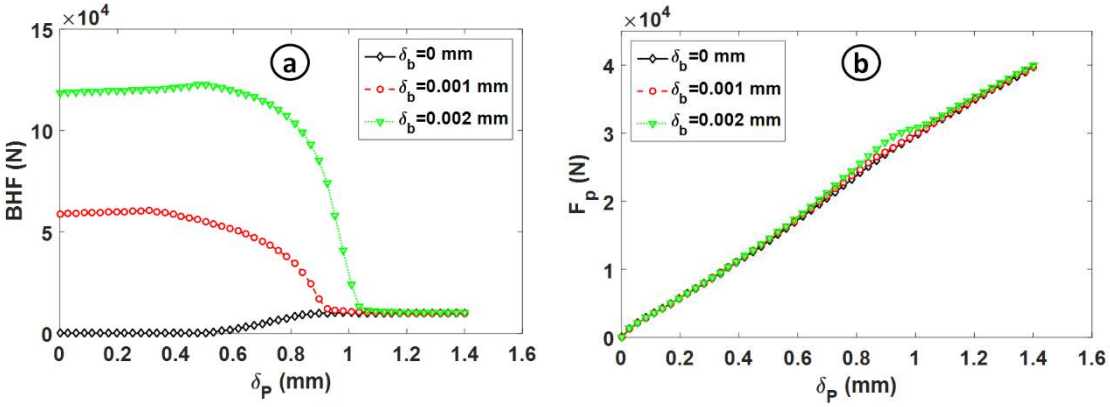


Fig.7 Evolution of loads versus the punch travel: (a) Blank-holder force; (b) Punch load, case (C1)

3.2.Analysis of forming kinematics and loads of case (C2)

In the industry, the progressive BHF is better applied simultaneously with the punch load during the countersinking process. To study the effects of progressive BHF on the forming kinematics, a first parametric study was conducted by varying E_S and using a nil clearance ($C=0$ *mm*); this is case (*C2*).

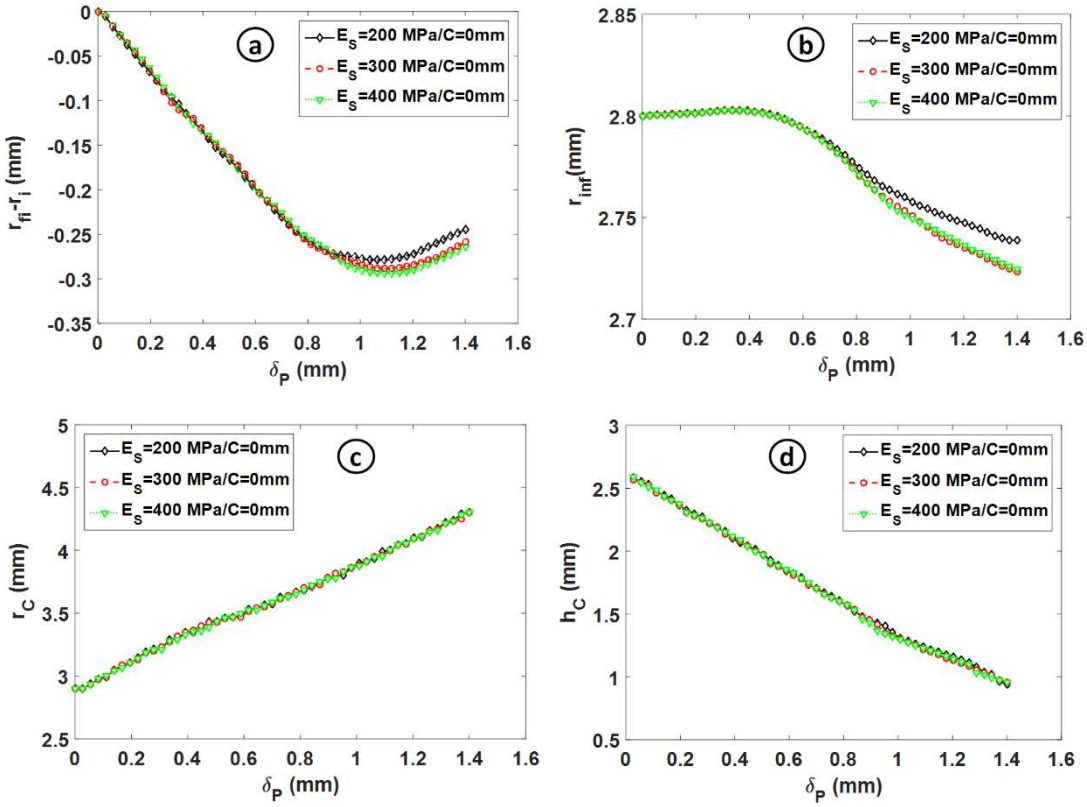


Fig.8 Evolution versus punch travel of :(a) Retraction, (b) R_{inf}, (c) r_C and (d) h_C , case (C2)

When E_S increased, the material flowed mainly in the direction of the inner hole of the workpiece. Consequently, the greater the E_S, the greater the retraction $(r_{fi}$-$r_i)$ and the inner diameter of the countersunk

hole r_{inf}, as shown in Fig.8-a-b. On the other hand, Fig.8-c-d shows that the variation of E_S did not affect the r_c and h_c.

In Fig.9-a, it can be seen that radial expansion is not influenced by E_S. In contrast, axial expansion increased clearly when using a greater value of E_S, Fig.9-b.

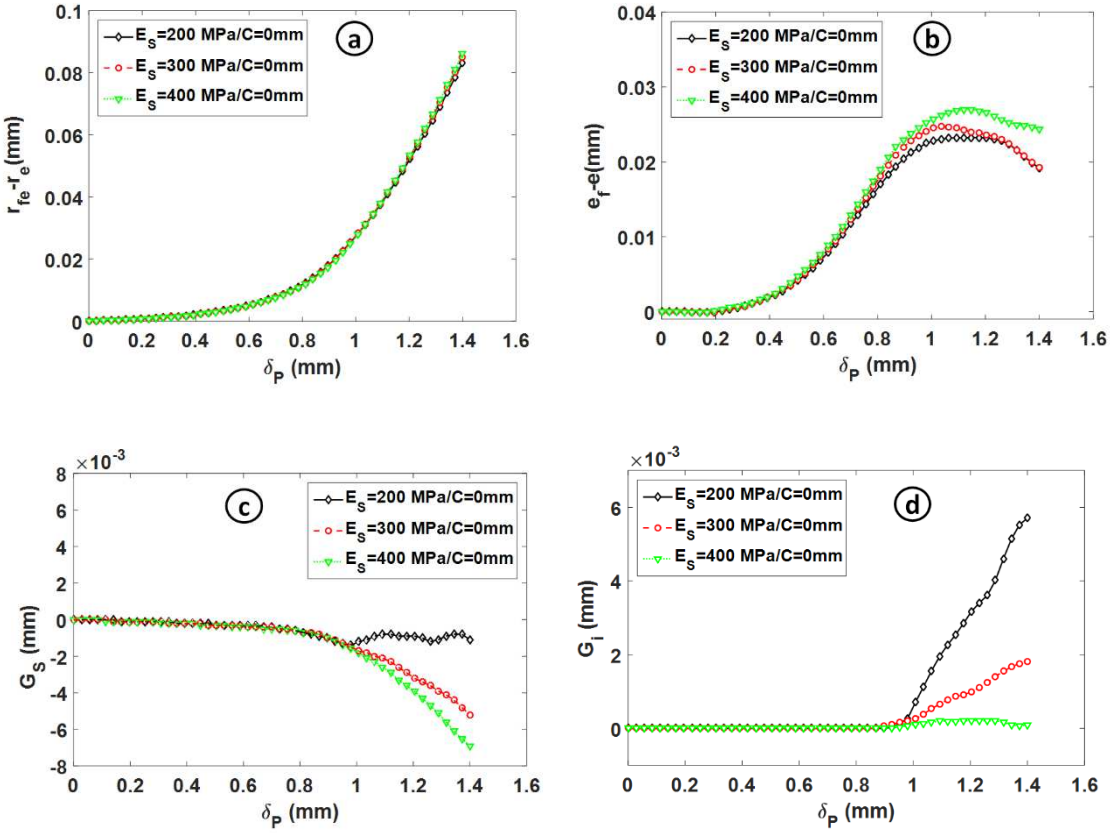


Fig.9 Evolution versus punch travel of: (a) Radial expansion, (b) Axial expansion, (c) G_S and (d) G_i, case (C2)

A greater E_S increases the progressive BHF, which pushes the workpiece into the die and prevents it from rising. As shown in Fig.9-c, the inferior gap G_i decreased from $6\mu m$, when E_S=*200MPa,* to approximately $0\mu m$, when E_S=*400MPa*.

Concerning the superior gap, it had two states: positive or negative. When E_S is low, the blank-holder couldn't support the force due to the rise of the workpiece. In this case, the superior gap is positive or nil. It is approximately equal to 0 µm when E_S=*200MPa* is used. With the increase in E_S, the BHF became greater than the reaction force, Fig10-b. As a result, the blank-holder pushed down the workpiece to prevent it from rising. Therefore, the superior gap G_s became negative and reached -7 µm when E_S=*400MPa,* as shown in Fig.9-d.

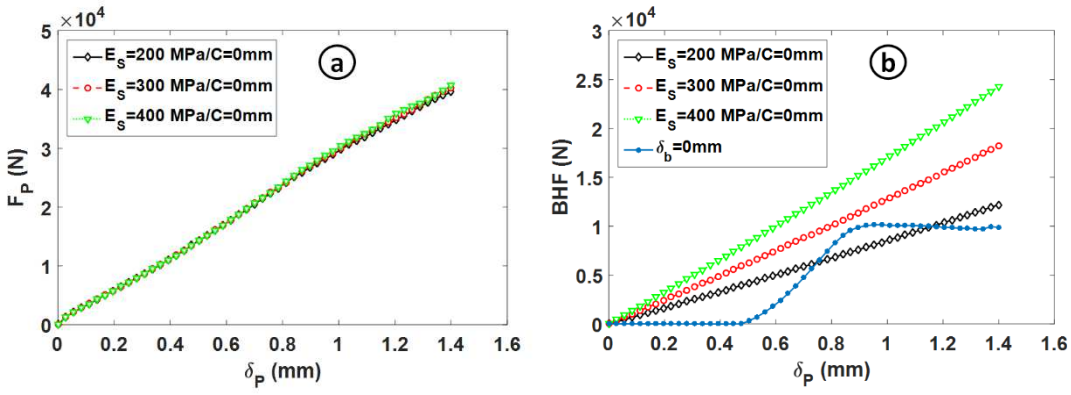


Fig.10 Evolution of the loads versus punch travel (a) Punch load, (b) Progressive BHF, case (C2)

The load evolution versus punch travel was plotted in Fig. 10-a. It can be noticed that progressive BHF did not influence the punch travel evolution and its final value, Fig.10-a. Since the annular ring is equivalent to an elastic spring, the resulting progressive BHF shows a linear evolution with the punch travel. Three types of progressive BHF curves were used: under, tangent, and above the reaction force curve, as shown in Fig.10-b. It is clear that the greater the E_S, the greater the final BHF.

As an exception, when E_S=*0MPa*, the BHF becomes zero, as if no blank-holder is above the workpiece: it is the case of countersinking without a blank holder. In this particular configuration, the inferior gap reached 37µm, as shown in Fig.11. This value was much greater than that obtained in cases (C1) and (C2), which affects the flatness of the workpiece. As a result, the use of a blank holder has a remarkable influence on the countersinking process. It reduces the appearance of inferior gap to achieve acceptable flatness of the sheet after forming, and enhances the retraction phenomenon. Therefore, the configuration without a blank holder was not detailed in this study.

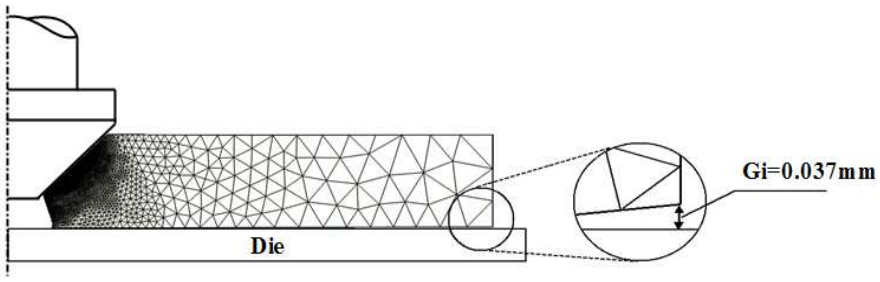


Fig.11 The inferior gap in the case of countersinking without blank holder

3.3. Analysis of forming kinematics and loads of case (C3)

The interesting use of the blank-holder was to conquer the reaction force by using a minimum BHF. Regarding the reaction force evolution, it was clear that the reaction force was nil until reaching 0.45 mm of punch travel. As a result, it was proposed to use a delay between the beginning of the punch load and the use of the BHF. This delay is achieved by using a clearance *C* between the blank-holder and the annular ring, as shown in Fig.3, this is the model of case (*C3*).

In Fig.12, it can be observed that retraction is clearly affected by progressive BHF: the greater E_S, the greater the retraction. Using a high stiffness led to a greater reduction in the final r_{fi}. On the one hand, the radial expansion was slightly affected by E_S despite the addition of the clearance C. On the other hand, axial expansion increased significantly when E_S increased.

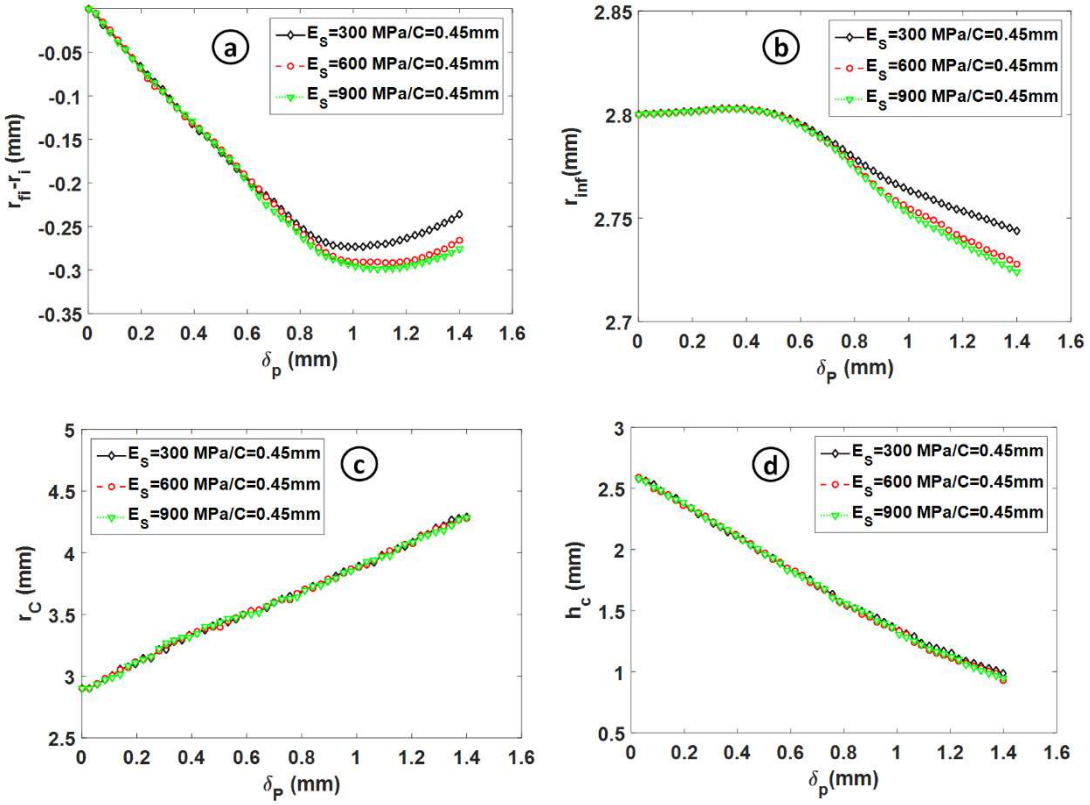


Fig.12 Evolution versus punch travel of: (a) Retraction, (b) R_{inf}, (c) r_C and (d) h_C , case (C3)

Referring to Fig.13, there are no significant deflections of the workpiece before the punch travel δ_p=*0.45mm*. The expansions and the gaps do not yet appear, or they are slight. After this delay is exceeded, the blank-holder applies a progressive load to the workpiece to prevent it from rising.

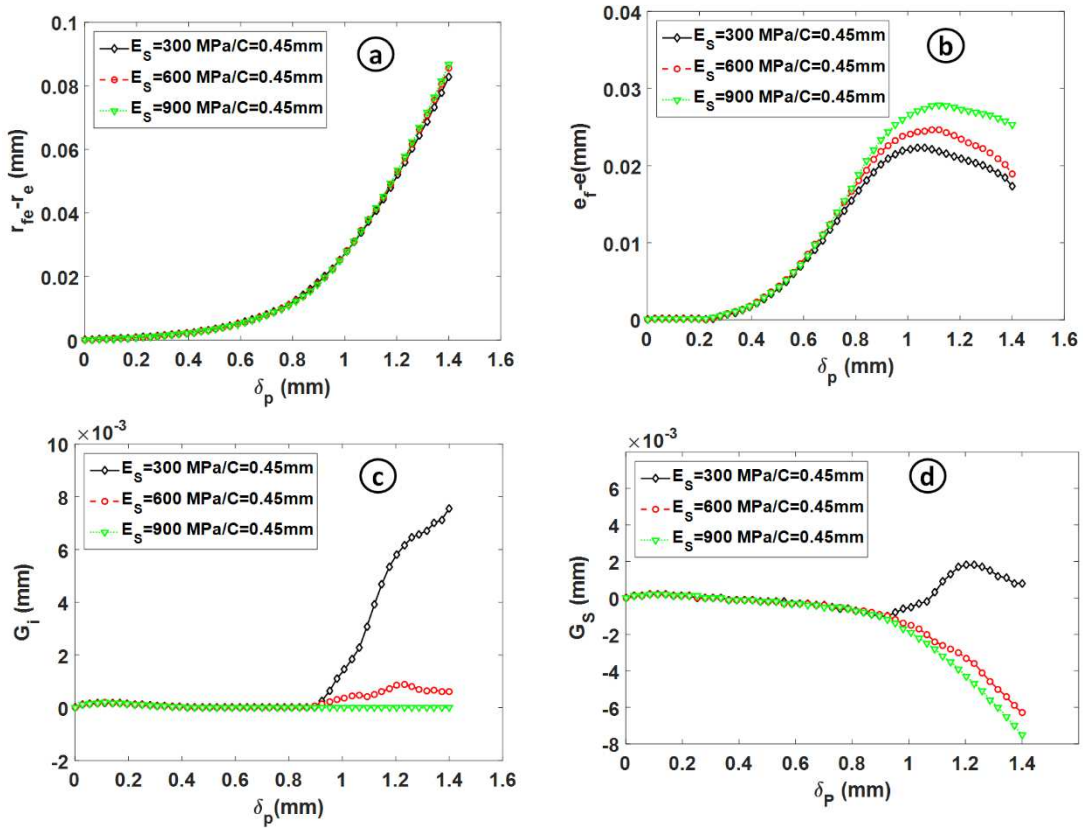


Fig.13 Evolution versus punch travel of: (a) Radial expansion, (b) Axial expansion, (c) G_S and (d) G_i, case (C3)

Fig.13-c-d shows that the greater E_S, the greater the superior gap G_s and the smaller the inferior gap G_i. It can be noted that when the BHF curve is under reaction force one (E_S=*300MPa*), the superior gap is positive. When the BHF curve is above reaction force one (E_S>*600MPa*), the superior gap becomes more negative, and the inferior gap decreases until reaching zero.

Therefore, E_S influenced retraction, gaps, and axial expansion. In contrast, the other parameters r_c, h_c, and radial expansion are not affected by it.

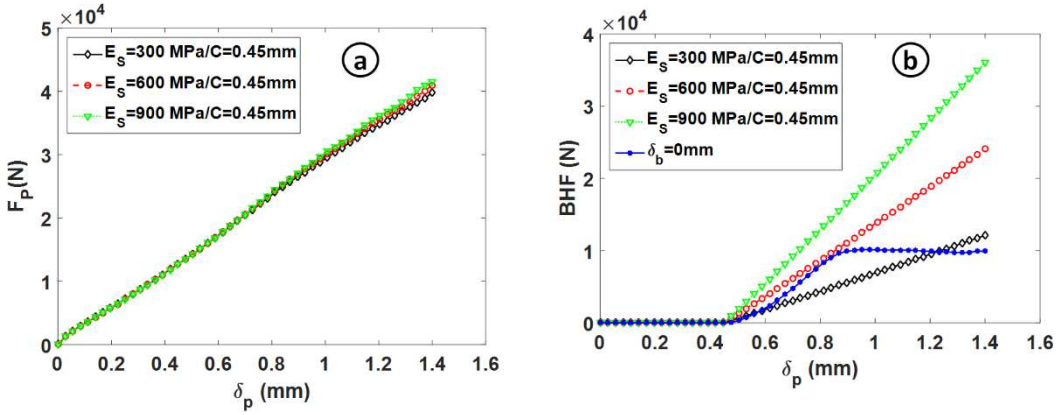


Fig.14 Evolution of the loads versus punch travel (a) Punch load, (b) Progressive BHF, case (C3)

In Fig.14, it is observed that the punch load was slightly affected at the end of the process. After the punch travel reached the value of *C=0.45 mm*, the progressive BHF appeared to prevent the workpiece from rising, as in case (C2). It was linear and proportional to the punch travel, as shown in Fig. 14.

3.4. Synthesis and comparison of the different cases

The three previous models were systematically compared to identify the optimal configuration for the countersinking process. The optimal solution is derived by minimizing energy consumption and workpiece deflections, ensuring enhanced efficiency and performance.

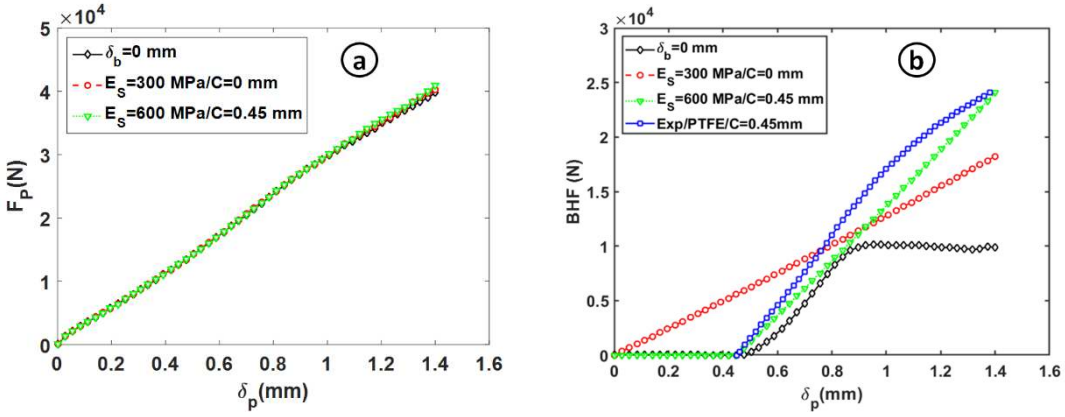


Fig.15 Comparison of load evolution for the three cases: (a) Punch load, (b) BHF and experimental BHF (PTFE)

For cases (C2) and (C3), the better configurations were obtained using, respectively, E_S *=300MPa* and E_S*=600MPa.* The evolution of the BHF for these two configurations is plotted in Fig.15-b. In case (C2), the maximum BHF is about *19 kN*, approximately equal to 45% of the punch load *of 41 kN*. In case (C3), the maximum BHF is *24 kN*, which is about 60% of the punch load. Referring to case (C1), when the imposed displacement is *1µm*, the obtained BHF is *59 kN*, about 144% of the required punch load for the countersinking process, as shown in Fig.7-a. As is known in manufacturing, the BHF force must always be smaller than the punch load. As a consequence, cases (C2) and (C3) can be used for manufacturing the countersunk hole, and case (C1) is rejected. For this reason, these two cases will be compared to the reference case (C1), when δ_b*=0µm*, to better choose between them and to understand the influence of the E_S and the clearance *C* on the forming kinematics and the loads.

The energy used for blank holding can be calculated as the area under the BHF curve. In Fig.16, case (C3) is the optimal configuration from an energetic point of view, when using E_S*=600MPa* and *C=0.45mm*. In addition, case (C2) could be the second-optimal model.

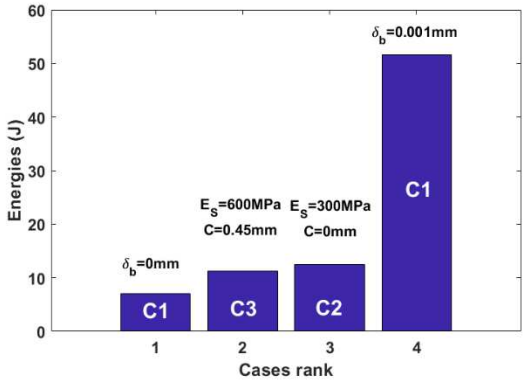


Fig.16 The energy used for the blank holding in the three cases (C1), (C2), and (C3)

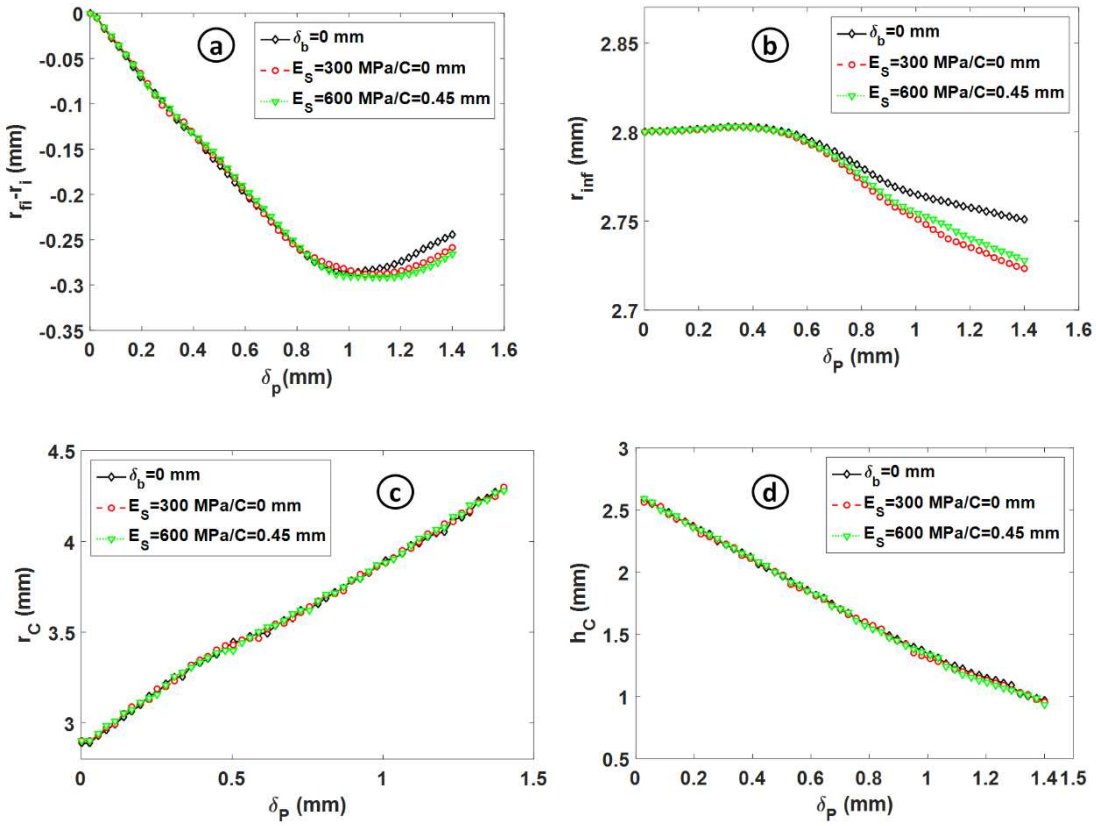


Fig.17 Comparison between the three cases: evolution of (a) Retraction, (b) R_{inf}, (c) r_c and (d) h_c versus δ_p

After analyzing the loads, the second interesting comparison concerns retraction. Fig.17-a shows that the retraction curves evolve in the same way for all three cases until a punch travel of *1mm*. After that, the utility of the elastic annular ring appeared, and retraction increased in cases (*C2*) and (*C3*) compared to case (*C1*) when δ_b=*0*μm. The inner inferior radius r_{inf} increased too, as shown in Fig.17-b. For the parameters r_c and h_c, the progressive BHF does not influence them, Fig.17-c-d

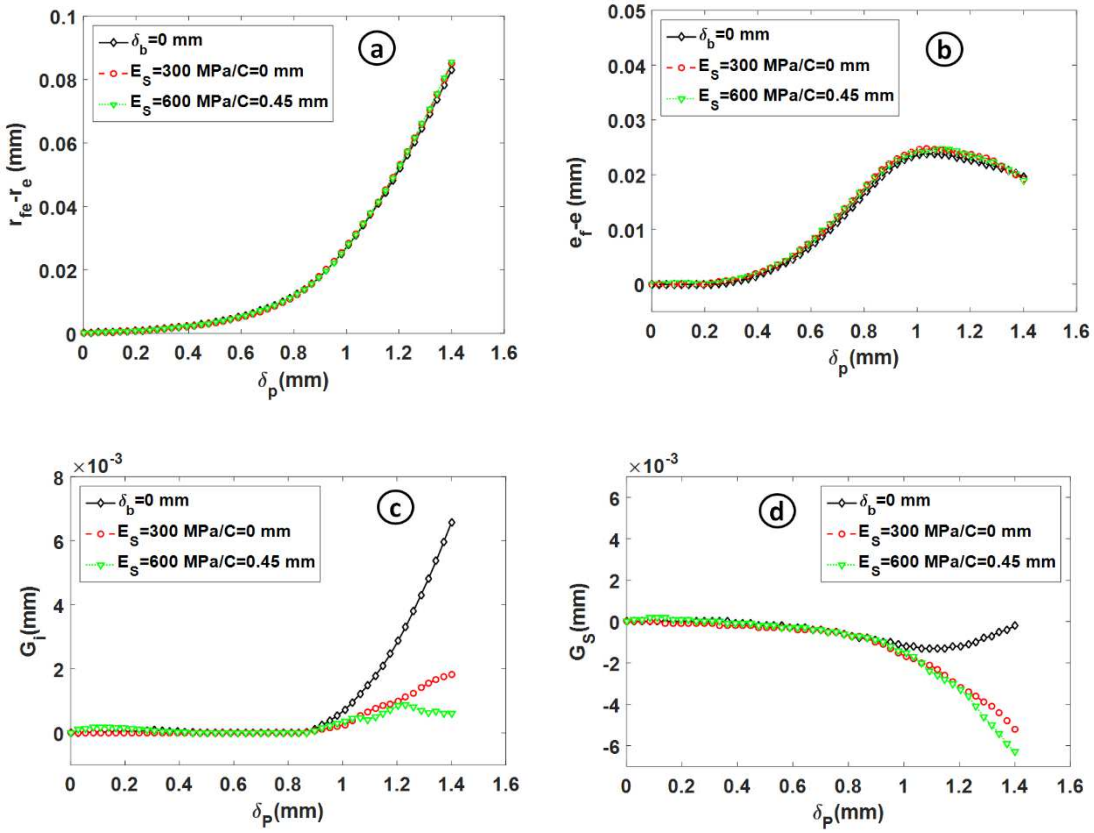


Fig.18 Comparison between the three cases: evolution of (a) Radial expansion, (b) Axial expansion, (c) G_S and (d) G_i, versus δ_p

Fig.18 illustrates the evolution of expansions and gaps during the countersinking process. It is observed that progressive BHF reduces the inferior gap G_i to one-third of its value in the reference case (C1) when δ_b=0μm. Conversely, there is an increase in the superior gap G_s. In cases (C2) and (C3), these gaps attained their maximum values at the end of the countersinking process.

As a consequence, the clearance C between the annular ring and the blank-holder only slightly affects the forming kinematics. In contrast, the stiffness of the annular ring has the dominant effect on the countersinking process. Finally, it can be concluded that model (C3) is the optimal one compared to case (C2).

3.5.Experimental results:

The experimental tests were conducted to validate numerical results and reveal the influence of the optimal case (C3) on the countersinking process. The workpiece was cut from the same sheet metal used to characterize the metal model, and it has, e=2.7mm, r_e=15mm, and r_i=2.8mm. In the numerical simulations, the annular ring was defined by E_S=600MPa and an equivalent stiffness K=2500N/mm. In practice, this E_S does not exist on the market. That's why a PTFE of E=540MPa was used to manufacture an equivalent annular ring with r_1=5.5mm, r_2=32mm and h=16.1mm. The obtained annular ring has approximately the same numerical stiffness K=25300N/mm. The clearance C=0.45mm was controlled by using the appropriate shim, as shown in Fig.4.

A compression test was performed on the annular ring to verify the experimental progressive BHF. In Fig.15-b, the evolution of this BHF is linear in the first stage of its appearance. After that, a curvature was noticed until the end of the test. This phenomenon can be explained by the expansion of the annular ring, which decreases the stiffness *K,* and thus the progressive BHF. The maximum difference between the experimental and numerical progressive BHF curves is about 14%. As a result, the experimental progressive BHF of this annular ring can be accepted.

In addition, the equivalent Von Mises stress S and the cumulative plastic strain PEEQ can be used to explain the forming kinematics in the different cases. As shown in Fig.19-a-b, blank holding using an imposed displacement leads to high values of S and PEEQ on the contact surface between the punch and the workpiece. In addition, a circular zone of PEEQ around the countersunk hole is observed; it is due to high contact pressure between the workpiece and the blank holder hole fillet. This phenomenon was seen in the experimental results as a circular scratch around the countersunk hole, as shown in Fig.19-c. Furthermore, axial expansion is clearly observed around the countersunk hole.

When progressive blank holding is used, the PEEQ decreased by 25% compared to the previous case (C1), Fig.19-e. In addition, axial expansion around the countersunk hole decreased, which enhances the flatness of the final surface, Fig.19-f.

It is worth noting that the numerical results demonstrated a good concordance with experimental data. As a consequence, the developed numerical FE models are validated and can be used to predict the loads and the forming kinematics of the countersinking process.

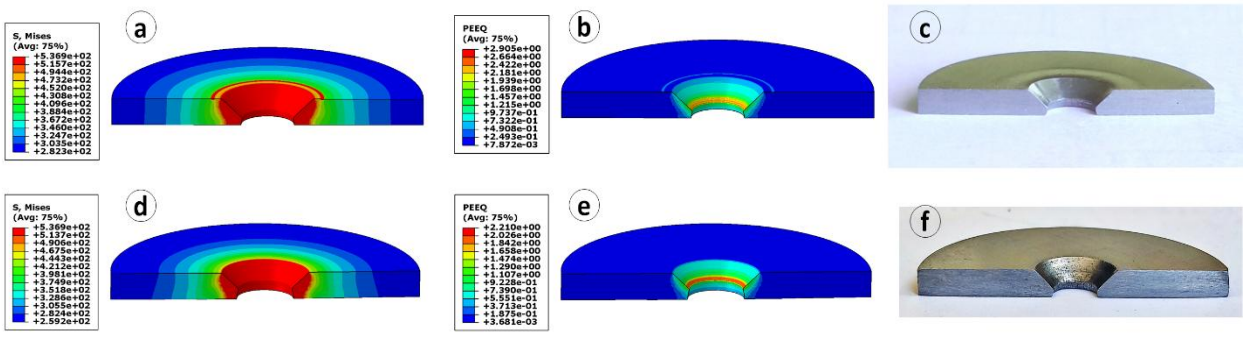


Fig.19 Case (C1) with $\delta_b=1\mu m$: (a) Von Mises stress, (b) PEEQ (c) Experimental cut view

Case (C3) with $E_S=600MPa$ and $C=0.45mm$: (d) Von Mises stress, (e) PEEQ (c) Experimental cut view

4. Conclusion

This study investigated the impact of blank-holder force on the forming kinematics and loads during the countersinking process. Three cases (C1, C2, and C3) were investigated using a numerical approach. The new cases (C2) and (C3) were compared with case (C1). Based on the analysis and the discussions, the main findings are summarized as follows:

- The FE models of these three cases were validated through direct comparison with the experimental results, establishing their reliability as a good tool to analyze the countersinking process.

- Case (C1), using an imposed displacement (δ_b=1μm) on the blank holder, led to an excessive BHF, exceeding the punch load by 40%, which makes this kind of blank holding unacceptable in manufacturing applications.

- Case (C2) involved the introduction of a progressive BHF from the initiation of the process, achieved through the incorporation of an annular elastic ring situated between the punch and the blank holder. The analysis indicated that the maximum progressive BHF was reduced and became 40% smaller than the punch load. This progressive BHF significantly influenced the process by enhancing retraction and reducing deflections, such as the inferior gap and axial expansion. In contrast, the punch load remained unaffected by this adjustment in BHF.

- Case (C3) was developed based on (C2). The primary distinction is the application of the progressive BHF after a delay from the initiation of the process, by using a clearance *C* between the blank holder and the workpiece. The resulting maximum BHF was 35% lower than the punch load. This progressive BHF influenced retraction, gaps, and expansion, while again demonstrating no impact on punch load.

- A comparative analysis of energy consumption associated with the blank holding revealed that while the influence of progressive BHF was approximately similar in both cases (C1) and (C2), the introduction of a clearance C resulted in a 10% reduction in energy usage in case (C3) compared to (C2).

- In manufacturing, the methodologies in cases (C2) and (C3) can be integrated into single-action punch machines, which are widely used due to their low-cost production.

The forthcoming objectives will concentrate on the optimization of the countersinking process through the application of progressive BHF, aiming to achieve standardized countersunk holes.

Declarations:

Ethics approval: 'Not applicable'
Consent to participate: Informed consent was obtained from all individual participants included in this study.
Consent for publication: All individual participants declare that they consent to the submission of this paper for publication
Authors' Contributions: This manuscript is a true original work.
Funding: 'Not applicable'
Competing Interests: 'Not applicable'
Availability of data and material: 'Not applicable'
Conflicts of interest: The authors declare no competing interests.
Code availability: 'Not applicable'

References:

1. Ray MS, Matthew IR, Frame JW (1998) Metallic fragments on the surface of mini-plates and screws before insertion, British Journal of Oral and Maxillofacial Surgery, Volume 37, pages:14–18

2. Urban M.R. (2003), Analysis of the fatigue life of riveted sheet metal helicopter airframe joints, International Journal of Fatigue, Volume 25, pages 1013–1026

3. Park C.Y., Alten F.G., Jung J.S. (2006), Stress intensity factors for surface cracks at countersunk holes, Engineering Fracture Mechanics, Volume 73, pages 1878–1898

4. M. Sohel Rana, C. Makabe, G. Fujiwara (2009), The effect of hole shape on the extent of fatigue life improvement by cold expansions, Engineering Failure Analysis, Volume 16, pages 2081-2090

5. S. Sathiya N., Pavan K., Satish C., Implication of unequal rivet load distribution in the failures and damage tolerant design of metal and composite civil aircraft riveted lap joints, Volume 16, pages 2255-2273

6. Jintong L., Anan Z., Yi L., Hulyue D, Yunbo B (2020), Numerical and experimental investigation on the rivet head flushness in automatic countersunk riveting. International Journal of Advanced Manufacturing Technology, Volume 110, Pages 395–411.

7. Park C.Y, Grandt A.F.Jr, (2007), Effect of load transfer on the cracking behavior at a countersunk fastener hole, International Journal of Fatigue, Volume 29, pages 146–157.

8. Chul YP., Alten F. (2007), Effect of load transfer on the cracking behaviour at a countersunk fastener hole. International Journal of Fatigue, Volume 29, pages 146–157

9. V. Blanchot, A. Daidie (2006), Riveted assembly modelling: Study and numerical characterization of a riveting process, Journal of Materials Processing Technology, Volume 180, Pages 201–209

10. Feras D., Mohammad G., Ghassan T., A modified equation for the stress concentration factor in countersunk holes, European Journal of Mechanics A/Solids, Volume 36, Pages 94-103

11. Hassen M., Jallouli I. Krichen A. (2017), Advanced analysis for the countersinking process, International Journal of Advanced Manufacturing Technology, Volume 90, Pages 3473–3481

12. Hassen M., Slimen A., Rachid N. (2020), Effects of the pre-hole geometry on the final shape of the countersunk hole, International Journal of Advanced Manufacturing Technology, Volume 108, Pages 1265–1274

13. Hassen M., Slimen A., Rachid N. (2021), Optimization of the countersinking parameters based on the response surface method, International Journal of Advanced Manufacturing Technology, Volume 117, pages 501–510

14. Jallouli I., Krichen A., Bougharriou A., Saï K. (2011), Finite element analysis of countersinking process. International Journal of Advanced Manufacturing Technology, Volume 55, pages 641–648

15. Zhao H., Gary G. (1996), The testing and behaviour modelling of sheet metals at strain rates from 10^{-4} to 10^{4} s^{-1}. Journal of Materials Science and Engineering, Volume 207, Pages 46-50.

16. Alves L.M., Nielsen C.V., Martins P.A.F. (2011), Revisiting the Fundamentals and Capabilities of the Stack Compression Test. Journal of Experimental Mechanics, Volume 51, pages 1565–1572.